RESEARCH ARTICLE

# Mesoscale modeling of coastal low-level jets: implications for offshore wind resource estimation

Christopher G. Nunalee and Sukanta Basu

Department of Marine, Earth, and Atmospheric Sciences, North Carolina State University, Raleigh, NC 27695, USA

## ABSTRACT

Detailed and reliable spatiotemporal characterizations of turbine hub height wind fields over coastal and offshore regions are becoming imperative for the global wind energy industry. Contemporary wind resource assessment frameworks incorporate diverse multiscale prognostic models (commonly known as mesoscale models) to dynamically downscale global-scale atmospheric fields to regional-scale (i.e., spatial and temporal resolutions of a few kilometers and a few minutes, respectively). These high-resolution model solutions aim at depicting the expected wind behavior (e.g., wind shear, wind veering and topographically induced flow accelerations) at a particular location. Coastal and offshore regions considered viable for wind power production are also known to possess complex atmospheric flow phenomena (including, but not limited to, coastal low-level jets (LLJs), internal boundary layers and land breeze–sea breeze circulations). Unfortunately, the capabilities of the new-generation mesoscale models in realistically capturing these diverse flow phenomena are not well documented in the literature. To partially fill this knowledge gap, in this paper, we have evaluated the performance of the Weather Research and Forecasting model, a state-of-the-art mesoscale model, in simulating a series of coastal LLJs. Using observational data sources we explore the importance of coastal LLJs for offshore wind resource estimation along with the capacity to which they can be numerically simulated. We observe model solutions to demonstrate strong sensitivities with respect to planetary boundary layer parameterization and initialization conditions. These sensitivities are found to be responsible for variability in AEP estimates by a factor of two. Copyright © 2013 John Wiley & Sons, Ltd.

## 1. INTRODUCTION

Offshore territories offer a number of advantages for wind power production such as reduced surface friction, space for larger turbine rotors, and close proximity to large population centers.[1–3] In 2011, Europe installed over 800 MW of off-shore wind energy bringing its total capacity to 3812.6 MW, nearly a 400% increase from 2007.[4] In Asia, China claims the largest national offshore wind energy infrastructure with 150 MW installed capacity as of the beginning of 2011.[5] In the USA, an offshore wind energy infrastructure has struggled to materialize because of political and social barriers. However, these challenges are expected to be overcome in the near future given the fact that abundant wind resources can be found relatively close to high energy consumption areas such as New York, Boston and Philadelphia.[6,7] As proof of this imminent development, over 2000 MW of capacity is currently in the planning and permitting process along the Mid-Atlantic and Northeast coastlines.[8] Similarly, the US West Coast also boasts high wind power potential and suitable bathymetry for the production of up to 75.5 GW of wind power off of the coast of California alone.[9] Despite its advantages, appeal and recent development, international offshore wind energy development is challenged by unique meteorological factors that are more or less negligible in the case of onshore development of the same size.

Similar to their onshore counterparts, offshore wind farms are designed to extract the maximum amount of wind power possible on the basis of local wind classifications. However, coastal and offshore wind regimes present a distinct suite of complex atmospheric processes that heavily dictate local wind climatologies and, in turn, wind power production.[10] Additionally, the accuracy of conventional wind resource assessments in these locations may be significantly constrained by limited observational data.[11] In coastal areas, the primary factors that induce these offshore atmospheric processes are attributed to the intrinsic thermal and roughness differences of water versus land.[12] The differences in heat capacity between water and land drives differential surface heating on a diurnal time scale at land/sea interfaces. This differential heating oftentimes forces circulations that manifest into propagating mesoscale frontal boundaries (e.g., land–sea breeze front). In some instances, these land–sea breeze fronts may be characterized by wind speed perturbations greater than 5 m/s.[13] Additionally, internal boundary layers (IBLs) can develop as synoptically driven surface winds adjust to differences in roughness as they traverse coastal boundaries; the effects of these flow adjustments can be evident up to 70 km from coastlines.[14] IBLs may also develop near sea surface temperature (SST) gradients associated with distinct oceanic currents; buoyant heterogeneities near these SST boundaries can lead to enhanced turbulence.[15] Potential offshore wind farm sites are also exposed to coastal low-level jets (LLJs), which are relatively narrow elevated channels of wind maxima. Although the dimensions of offshore LLJs have not been fully documented, onshore LLJs are typically bounded between ~100 m and ~1000 m above ground level (AGL) and span a width of ~100 km.[16,17] Similar to onshore LLJs,[18,19] offshore LLJs are also expected to transport moisture, heat and other scalars (i.e., passive, active and reactive) hundreds of kilometers. In addition to these mesoscale atmospheric phenomena, other types of phenomena on different scales, such as hurricanes and waterspouts, may also influence offshore wind energy development.

Given the current lack of offshore wind measurements at hub height, the necessity for computationally modeled wind climatology data is significant.[6,8] Despite this necessity, atmospheric boundary layer (ABL) simulations intended for a variety of applications, including but not limited to wind energy, have been shown to be heavily sensitive to planetary boundary layer (PBL) parameterization. This sensitivity is also known to be amplified when complex mesoscale atmospheric processes are involved.[20–24] Recent coastal and offshore mesoscale modeling efforts devoted to wind resource assessment typically employ a standard PBL scheme for all simulations regardless of the atmospheric features commonly present in their computational domain. In this paper, we provide evidence of the diversity in coastal mesoscale model solutions attributed to PBL parameterization. We also advocate for the use of ensemble physics (i.e., the consensus of multiple physics schemes[25]) when simulating diverse coastal mesoscale phenomena for offshore wind resource estimation.

In summary, mesoscale atmospheric phenomena are particularly relevant to offshore wind energy both from productivity and sustainability perspectives. The motivation for this paper is rooted in the fact that the limitations of modern numerical mesoscale models are not well understood with respect to these offshore phenomena. To partially address this knowledge gap, we will focus on a single phenomenon, the coastal LLJ.[*] The coastal LLJ is chosen above other processes because, similar to onshore LLJs, it can be especially influential in affecting wind power production and is often overlooked.

The content of this paper is as follows: in Section 2 we discuss the state-of-the-science concerning onshore and offshore LLJs. Section 3 outlines a specific offshore LLJ case study used for model validation and summarizes the details of the mesoscale modeling system. Modeled results are presented and compared with observations in Section 4 while model solution sensitivities are identified with respect to specific modeling components. Section 5 summarizes the key results from this study. Finally, in Section 6 we discuss the implications of our findings and directions for future work.

## 2. BACKGROUND

The characteristics which define an LLJ lack scientific precision, and many different definitions have been suggested over the past 60 years. While establishing an LLJ climatology for the Eastern US and Great Plains, Bonner et al.[26] defined an LLJ as a wind maximum below 1.5 km AGL and having a peak wind speed of greater than 12 m/s with a 50% decrease in wind speed above the maximum (but below 3 km AGL). Many years later, Whiteman et al.[27] modified the definition of Bonner et al.[26] to allow weaker jets (i.e., with wind maximum less than 12 m/s) to also be classified as LLJs. Additionally, Song et al.[28] further modified the definition of Whiteman et al.[27] and defined the maximum height of LLJs to be below 2 km AGL (as opposed to 3 km AGL). Vastly different from each of these classifications, Andreas et al.[29] and Banta et al.[16] put forth a more relaxed definition of LLJs and characterized them as having wind speed decreases of 2 and 1.5 m/s (respectively) both above and below a wind maximum of any intensity. As exemplified by the diversity of each of these definitions, to classify a particular phenomenon as an LLJ can sometimes be a subjective process. It is for this reason that in this paper, we have selected to study an event that appears to abide by all popular LLJ definitions.

Before investigating the ability of a conventional mesoscale model to simulate coastal LLJs, it is important to understand the fundamentals of LLJs and the conditions that spawn them. For this reason, it is necessary to review the recent studies

---

[*]Here, we use the terminology coastal LLJs and offshore LLJs interchangeably. In both cases, we are referring to LLJs associated with land–sea interfaces, which may be positioned completely, or partly, over land or sea.

and findings related to offshore LLJs. However, considering the lack of literature pertaining explicitly to offshore LLJs, we will also review material concerning onshore LLJs as they are expected to share similar characteristics.

## 2.1. Onshore low-level jets

To date, the majority of scientific studies related to LLJs have focused primarily on onshore nocturnal jets. Through these investigations, much has been learned about the inherent features of LLJs and their implications for wind energy.[22,30,31] Aside from the obvious advantage of boosting nighttime wind power production, LLJs are capable of producing enhanced low-level (~100–200 m AGL) turbulent kinetic energy (TKE) through shear instabilities.[32,33] Observational data from field studies such as the CASES99 experiment in the US Great Plains[34] support the hypothesis that strong turbulence could be generated aloft near the jet core and then mixed downward.[16] This enhancement of turbulence beneath LLJs, which is introduced into the nocturnal stable boundary layer, can threaten the sustainability of modern wind turbine blades, which are not designed with bursting turbulence in mind.[35] Also, enhanced ABL turbulence has been documented to degrade wind turbine efficiency.[36]

Onshore LLJs are hypothesized to be invoked by a number of different atmospheric mechanisms such as inertial oscillation,[37–39] differential surface heating[40] and diurnal thermal wind balance associated with sloping terrain.[38] Bonner[26] first collected observational data from the US Great Plains LLJs and found them to occur over 60% of the nights. More recently, other LLJ climatology studies have been conducted using records collected by meteorological masts, sodars and wind profilers;[27,28,41,42] some of these studies found warm season LLJ events to occur more frequently than cool season events in the US.

## 2.2. Offshore low-level jets

The characteristics of offshore LLJs are much more elusive than onshore LLJs because of a relative lack of observations. The maritime environments that support offshore LLJs have a distinctly weaker diurnal stability cycle compared with onshore environments.[43] They have also been observed to yield vertical wind speed gradients greater than predicted by the standard Monin–Obukhov similarity theory.[2] This is especially important for wind energy applications because the LLJs that develop offshore may be closer to the surface than onshore LLJs. For example, in the Baltic Sea, LLJs have been documented as low as 30 m above sea level in stably stratified boundary layers.[44] Although the characteristics of offshore and onshore LLJs may be similar in some regards, the formation mechanisms of offshore LLJs are sometimes different from onshore LLJs.

In the early 1990's Doyle and Warner[45] studied an offshore LLJ event along the Carolina coastline, which appeared to have been initiated by geostrophic forcing in a narrow baroclinic zone. This study found the jet height and intensity to be sensitive to both surface flux modifications and latitude. On the other hand, other studies of offshore LLJs[46] in the same region found that the sloping terrain related to the Appalachian mountain chain, which essentially runs parallel to the coastline, may also aid in US East Coast LLJ formation. Yet even more recently, the common summertime US East Coast LLJ was hypothesized to be most typically initiated by the differential surface heating associated with the highly fluctuating ground temperatures onshore and the adjacent steady ocean surface temperatures.[47] In another part of the world, Jiang et al.[48] studied a Pacific Ocean LLJ off the coast of Chile and concluded that geostrophic forcing, coupled with baroclinic amplification induced by the Andes mountains and differential surface heating, were critical components to the jet's existence and behavior. Near the northern German coastline, four nocturnal LLJs were observed during the PUKK experiment; from these observations, Kraus et al.[49] documented one of these jets to have been associated with the familiar onshore formation mechanism known as inertial oscillation.[37]

Another less popular yet equally plausible coastal LLJ formation mechanism is based on the theory of Hsu.[50] This theory states that coastal LLJs can develop between mesoscale elevated inversions and nocturnal microscale ground-based inversions. This scenario may be established through nighttime radiational cooling and can induce an LLJ as a result of both Venturi and gravity–wind effects.[50] A criteria of this formation mechanism is that the oversea air temperature should ideally differ from the adjacent overland temperature by more than 5 °C since this allows the land surface cold pool to form.[51,52] From a wind energy perspective, this theory is important because it supports the possibility of very low LLJs (<100 m AGL) within ~20 km of global coastlines (this is the region along which the near-surface thermocline is most significantly sloped and gravity-effects are maximized). All in all, literature from past years has indicated that many coastal jets may form because of a combination of dynamics, which in some cases may act harmoniously with one another.

## 2.3. Offshore low-level jet climatology

Many studies have been devoted to studying the climatology of inland LLJs.[16,26–28,42] Findings from these studies have exposed the fact that LLJ activity is not a rarity and can be quite common in certain favored locations (i.e., the U.S. Great

Plains are known to experience LLJs up to 60% of the nights). On the other hand, studies documenting the frequency of coastal LLJs are much fewer. Nonetheless, in their global nocturnal low level jet index, Rife *et al.*[53] highlighted the presence of increased LLJ frequency in certain coastal regions around the world; the Eastern US being one of them. Additionally, Zhang *et al.*[46] studied specifically the US Mid-Atlantic LLJ jet and found it to have a magnitude of 8–23 m/s with a mean height of 670 m AGL and a frequency of 15–25 days per month during the warm season. Similarly, Ryan[54] found jets over Maryland of durations equal to or greater than 2 hours to occur on 43% of days with a mean intensity of 14 m/s. Also, Colle and Novak[47] found LLJs near the New York Bight to have typical magnitudes between 11–12 m/s at a height of only 29 m above sea level as measured by buoy wind speed sensors.

The information provided by the aforementioned studies, coupled with the known LLJ formation mechanisms previously discussed, lead the authors to believe that coastal LLJs along the US East Coast are common enough and strong enough to be influential to offshore wind energy development and performance. To support this assumption, a preliminary climatology study was conducted mainly to assess the annual number of occurrences of coastal LLJs in the Northeastern US coastal region. This climatology used hourly windspeed data from the RUTNJ vertical wind profiler (see Section 3) to document the frequency, magnitude and height of LLJs that occurred in that region throughout 2010. It was found that coastal LLJs occur over the RUTNJ profiler at least 118 days out of the year (i.e., 32%) with a mean magnitude of ∼15 m/s and mean height of ∼525 m AGL. A vertical wind profile was considered to have an LLJ signature when a clearly discernible wind maxima was present for at least two samplings (i.e., 2 hours) with at least a 4 m/s decrease in wind speed both above and below the jet core. The magnitude of an LLJ was taken to be its highest wind speed maxima recorded by the profiler, and its height was the height at which its peak wind speed occurred.

We feel that the statistical estimates yielded from this simple study are extremely conservative and open to a number of sources for error: (i) our LLJ criteria was fairly strict (compared with[16,29]), (ii) the data set was not free of data gaps (i.e., many LLJ events may not have been captured by the profiler), (iii) the profiler was unable to capture very low LLJs as profilers do not record measurements within about the lowest 100 m AGL and (iv) the coarse data set sampling interval (1 hour) makes classifying average LLJ magnitude and height potentially biased considering their temporal morphology. Additionally, it should be noted that the year selected for analysis may or may not have been meteorologically representative of a typical year. Nonetheless, this brief coastal LLJ climatology investigation indicates that the LLJ studied in this work is characteristically not an outlier for the region and that offshore wind energy developers can expect similar LLJ activity to occur about 1 out of every 3 days or more.

## 3. DATA AND METHODOLOGY

In this study, a prominent coastal LLJ event (July 15–17, 2011) was identified on the basis of observational data provided by two 915 MHz MADIS vertical wind profilers along the US Northeastern Seaboard (RUTNJ in New Brunswick, NJ and BLTMD in Beltsville, MD) and a radiosonde (OKX) from Upton, NY (Figure 1 left panel). Profilers, such as RUTNJ and BLTMD, have been previously used to identify and analyze similar Mid-Atlantic coastal LLJs with reasonable accuracy.[54,55] The MADIS profilers used in this study provide wind speed and direction data for heights between ∼100 m
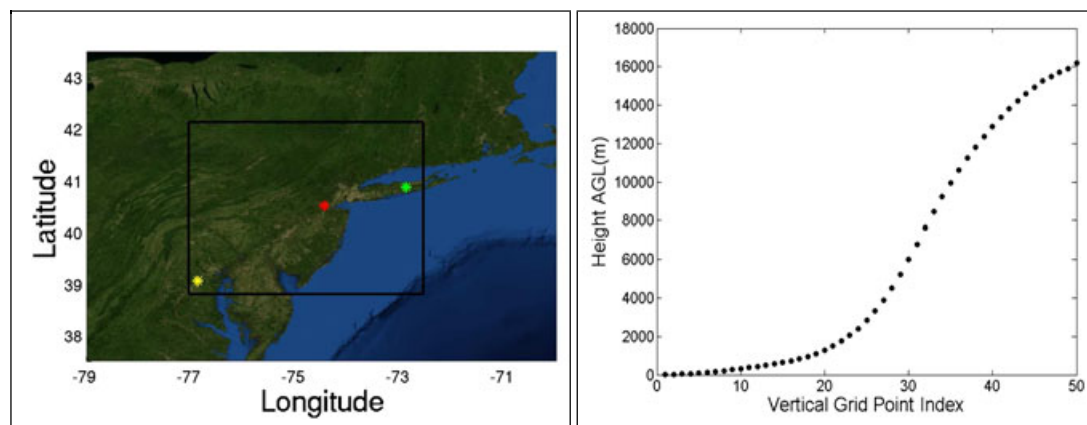


**Figure 1.** (Left) WRF d03 modeling domain (black rectangle) along with observational data sources (RUTNJ, 40.50 N/74.45 W, red star; BLTMD, 39.0554 N/76.8785 W, yellow star; OKX, 40.8694 N/72.8867 W, green star). (Right) Vertical grid point density as a function of height.

and ∼2000 m AGL and have a temporal resolution of 10 minutes. The radiosonde provided wind and temperature profiles at 00Z and 12Z each day at about seven vertical heights below 1 km AGL. The quality control procedures for these data sets are provided in the National Weather Service Technique Specification Package.[56] Observational data from the profilers and radiosonde were used to verify version 3.3 of the Weather Research and Forecasting model (WRF) while simulating the identified LLJ event.

The WRF model is a non-hydrostatic mesoscale numerical weather prediction model used extensively within academia, government and industry. The WRF model is capable of simulating a plethora of synoptic scale, mesoscale and microscale atmospheric phenomena and is equipped with multiple parameterization schemes (e.g., micro-physics, land-surface inter-action, radiation, planetary boundary layer, etc.).[57] To evaluate the performance of the WRF model's PBL parameter-ization options in simulating this offshore LLJ event, WRF was run multiple times over the US East Coast domain for the dates of the LLJ event occurrence. For each model run, a different PBL parameterization was invoked while all other model configurations were held constant. The various PBL schemes evaluated here were Yonsei University,[58] Mellor–Yamada–Janjic,[59] Quasi-Normal Scale Elimination,[60] Mellor–Yamada Nakanishi and Niino Level 2.5,[61] Asym-metric Convective Model,[62,63] and BouLac.[64] Other parameterization schemes used in these simulations were WRF Single-Moment 5-class Microphysics,[65] RRTM Longwave Radiation,[66] Dudhia Shortwave Radiation,[67] Kain–Fritsch Cumulus[68] and the Noah Land Surface Model.[69]

## 3.1. Modeling domain configuration

For all LLJ simulations, the WRF model's preprocessing system (WPS) was used to construct a nested numerical modeling domain centered on the location of the RUTNJ vertical wind profiler. This domain configuration consisted of a large parent domain with two nested domains. The outer domain, d01, employed an 18 × 18 km horizontal resolution; the intermedi-ate domain, d02, used a horizontal resolution of 6 × 6 km and the target domain, d03, encompassed the observation sites and operated by using a horizontal grid resolution of 2 × 2 km (Table I). Throughout all the domains, the vertical resolu-tion remained constant with 50 grid points between the surface and 16,000 m AGL, the lowest of which was ∼8 m AGL (Figure 1 right panel). About 18 out of the 50 total vertical grid points were below 1 km. Land use and topographical prop-erties for these simulations were taken from the US Geological Survey at resolutions comparable with the grid resolution. Model runs were executed for a total of 96 hours with the first 24 hours being used as spin-up time for the simulations. The simulations operated using a 90 second integration time step on d01, a 30 second time step on d02 and a 10 second time step on d03. Model output was extracted for analysis every 10 minutes for d03. Standard wind resource models use slightly lower vertical resolutions and about the same horizontal resolutions.[70] Operational numerical weather prediction models, on the other hand, have a much coarser horizontal resolution but about the same vertical resolution.[71] Appendix A contains a detailed study of the effect of vertical resolution on accurate offshore LLJ simulation.

## 3.2. Model initialization

Similar to all computational fluid dynamics models, the WRF model requires initial and boundary condition data to initiate and time integrate atmospheric simulations. For the case study presented here, the WRF model was prescribed mete-orological initialization conditions from the ERA-Interim and North American Regional Reanalysis (NARR) data sets. ERA-Interim is a data assimilation system produced by the European Centre for Medium Range Weather Forecasts and contains environmental data records from 1979 through the present at 6 hour intervals. The ERA-Interim data set includes a horizontal resolution of approximately 79 km and 60 vertical coordinate levels.[72] NARR is produced by the National Centers for Environmental Prediction and is similar to ERA-Interim; however, its geographic coverage only encompasses North America. The NARR data set has a horizontal resolution of approximately 32 km with 42 vertical levels.[73] As will be discussed, model initialization data appears to have a substantial influence on the WRF model's wind output (see Section 4.2). Ultimately, ERA-Interim data were chosen for most of the analysis in this paper as it allowed the WRF model to capture the LLJ event much more accurately.

**Table I.** Domain Configuration.

| Domain | Δx | Δt | Nx | Ny | Domain Size |
|--------|------|------|-----|-----|----------------------|
| d01 | 18 km | 90 s | 100 | 100 | 1782 km × 1782 km |
| d02 | 6 km | 30 s | 181 | 181 | 1080 km × 1080 km |
| d03 | 2 km | 10 s | 181 | 181 | 360 km × 360 km |

## 4. RESULTS

During July 14–17, 2011, the US Northeastern Seaboard experienced a relatively uneventful synoptic-scale atmospheric pattern. Surface high pressure, centered off of the coast of Virginia, persisted throughout the majority of the period, preventing the encroachment of any large-scale weather system (Figure 2 upper left panel). Based on modeled data, the individual nocturnal LLJs that developed during this time frame were oriented parallel to the US northeastern coastline with a crosswise width of about 100 km and a streamwise length of about 1000 km (Figure 2 upper right panel).

The initiation of the three consecutive LLJs could easily have been due to a combination of multiple atmospheric processes. Of note, the geostrophic flow was from land to sea and fairly weak (Figure 2 bottom row) throughout the event. This was ideal forcing for the jet formation mechanism outlined by Hsu[50] as the offshore pressure gradient could have potentially amplified PBL winds in a baroclinic zone near the coast as they were decoupled from the surface at night. Furthermore, the event took place in July when the SST were generally warmer than the adjacent nighttime overland temperatures. This temperature difference likely played a significant role in jet formation because of the across-shore changes it induced to the near-surface microscale cold pool. In addition, other mechanisms common for onshore LLJs, such as sloping terrain, may have contributed to the formation of these coastal LLJs. On the other hand, inertial oscillation, which is a very common onshore LLJ formation mechanism, was not observed in the measured hodographs from RUTNJ and BLTMD.
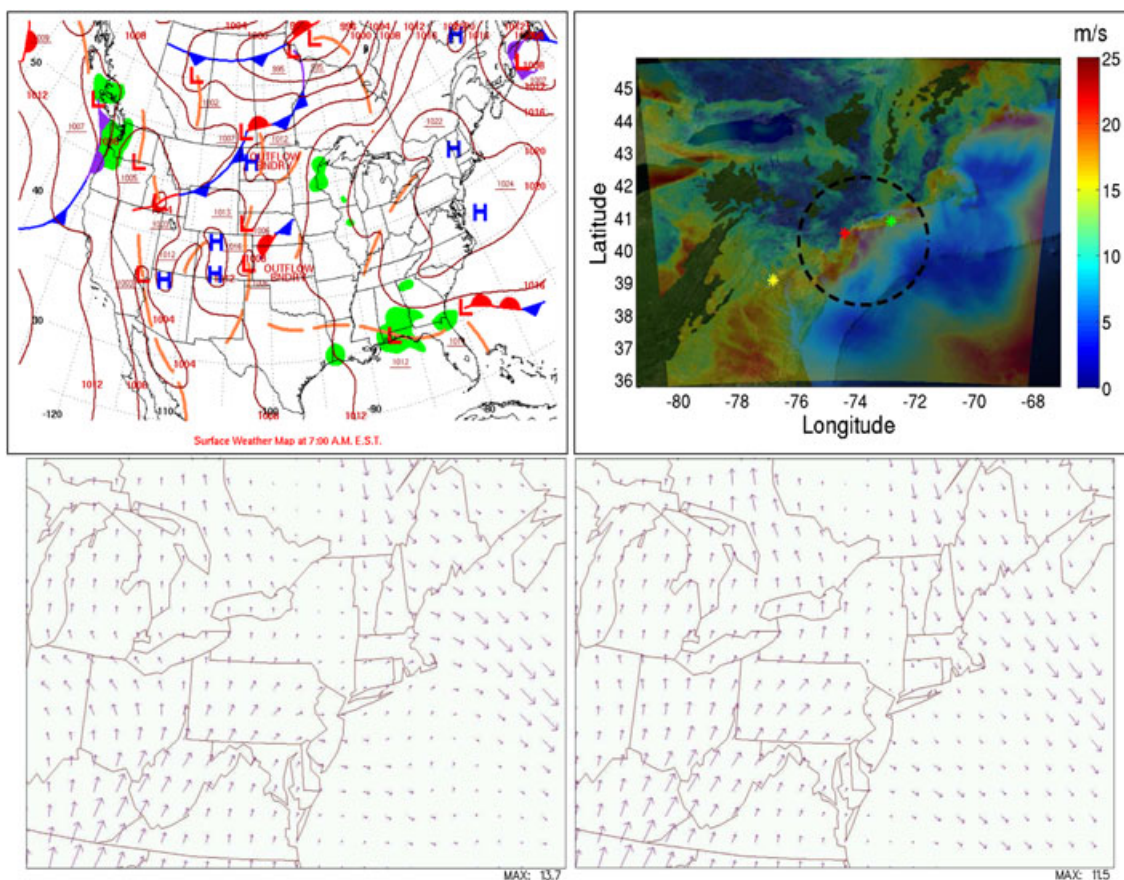


**Figure 2.** The Eastern US seaboard was dominated by a synoptic-scale surface high pressure system on 7/16/2011 as shown by the Hydrometeorological Prediction Center surface analysis (upper left). A plan view of 300 m AGL wind speed displays the coastal LLJ (outlined in black) along the northeastern US seaboard as simulated by the WRF model valid 0Z (upper right). Wind data is masked over areas where the terrain height is greater than 300 m AGL and verification data source locations are labeled the same as in Figure 1. 1000 mb geostrophic wind vectors also show the weak offshore geostrophic forcing along the US Northeastern coastline at 00Z 7/16/2011 (bottom left) and 12Z 7/16/2011 (bottom right). Geostrophic wind figures were provided by Plymouth State Weather Center; value of maximum vector size (m/s) is indicated beneath each figure.
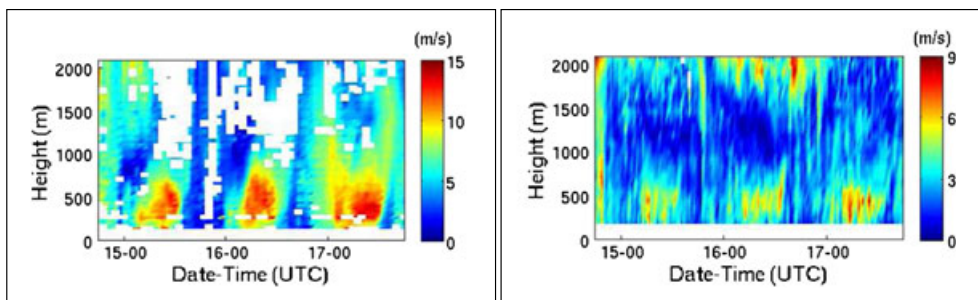
**Figure 3.** Time versus height plots of wind speed observations from the RUTNJ (left) and BLTMD (right) MADIS vertical wind profilers during July 14–17, 2011. Note that the color scale of the BLTMD plot has been adjusted to reflect weaker wind maxima.
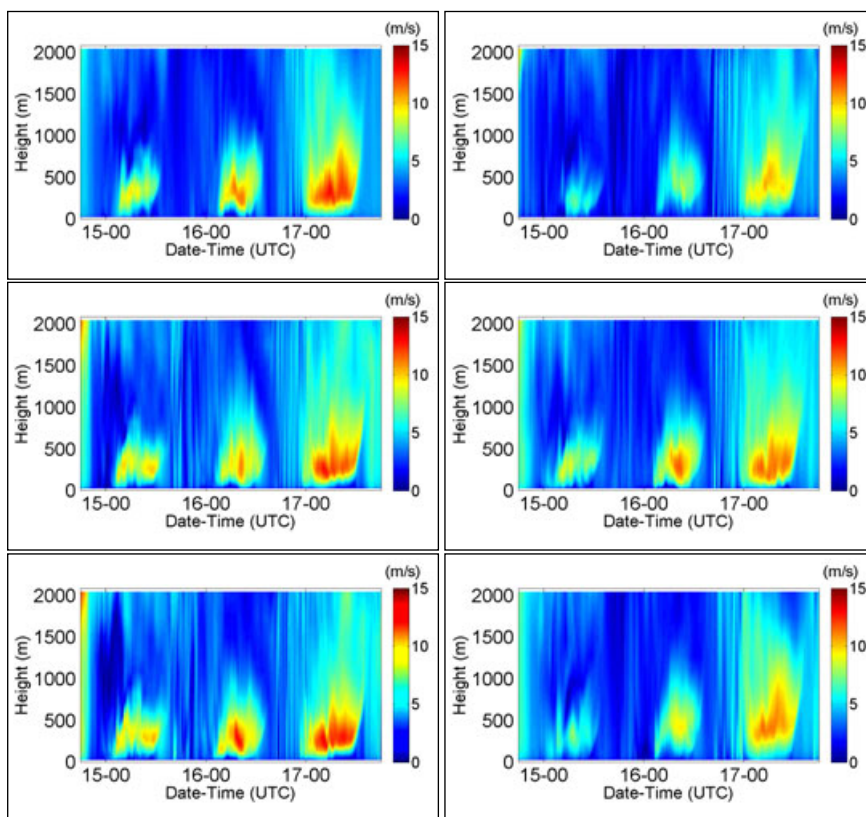


**Figure 4.** WRF model-derived time versus height plots of wind speed during July 14–17, 2011 at RUTNJ using ACM2 (top left), BLc (top right), MYJ (middle left), MYNN2 (middle right), QNSE (bottom left) and YSU (bottom right).

Wind speed observations from the RUTNJ profiler (Figure 3 left panel) display the structure and temporal evolution of three consecutive nocturnal LLJs. The three jets were observed on the nights of July 15th, 16th and 17th between roughly 00UTC and 12UTC. The timing of each jet's development and disappearance, along with their vertical limits (∼100–800 m AGL), is fairly consistent throughout all nights. Nevertheless, the intensity and core structure of each jet varies throughout the event. The LLJ that occurred on July 17th was the most intense with peak wind speeds greater than 15 m/s over RUTNJ. Although the BLTMD profiler site was not directly beneath the jet cores, it did record weak LLJ signatures on each of the three nights (Figure 3 right panel).
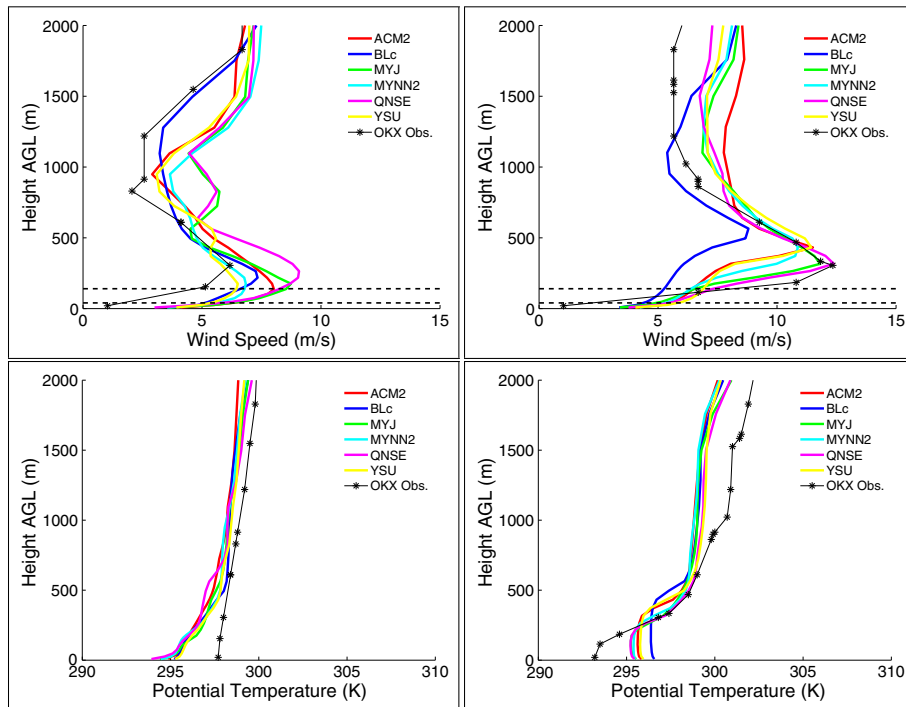
**Figure 5.** Wind speed (top row) and potential temperature (bottom row) as a function of height for the OKX radiosonde launch site. Modeled profiles are colored and sounding observations are denoted by a line with stars. Data valid July 16, 2011 00Z (left column) and July 17, 2011 12Z (right column). Dashed black lines represent typical wind turbine rotor plane top and bottom heights (40 m and 140 m AGL).

### 4.1. Sensitivity to planetary boundary layer parameterization

Individual PBL schemes within the WRF model simulated the series of Northeastern US coastal LLJs with noticeable diversity. Figure 4 illustrates the fact that each PBL scheme struggled to capture the intensity and structure of each of the LLJs; however, the timings and vertical bounds of each jet feature were modeled reasonably well. The MYJ, ACM2 and QNSE PBL schemes simulated the most intense, and most accurate, coastal LLJ event with maximum winds approaching 15 m/s for the final jet.[*] The initial nocturnal jet was the weakest and the most difficult for each scheme to represent.

#### 4.1.1. Wind speed and potential temperature profiles.

Validation using radiosonde profiles also show interesting qualities of the WRF–PBL schemes. When compared with observations at 00Z on July 16th, it is evident that all PBL schemes overpredicted the LLJ's intensity and underpredicted its height, with the MYJ and QNSE schemes performing the poorest (Figure 5 left column). Also at this time, the near surface modeled atmosphere has a cold potential temperature bias. Nevertheless, looking at the jet that occurred on July 17th at a later time, the MYJ and QNSE schemes most closely match the shape of the wind speed profile (Figure 5 right column). At this same instance, other PBL schemes overestimated the height of the jet core (~300 m AGL) and underestimated its maximum intensity (~13 m/s). The BouLac scheme was the most extreme in its intensity underestimation with an error of about 4 m/s. On the other hand, wind speeds above the LLJ were unanimously overestimated by all schemes. With regards to potential temperature correlation, simulation results were consistent throughout the boundary layer and free atmosphere (Figure 5); however, there was a warm thermal bias near the surface below ~300 m AGL.

#### 4.1.2. Wind speed distribution.

The diversity among PBL schemes translates to non-negligible differences in the wind resource characterization at particular locations. To quantify these differences, the modeled 3 day wind speed distributions for 179 m AGL at the RUTNJ site are compared with the observed wind speed distribution in Figure 6. It is evident that all schemes underestimated

---

[*]During the course of the current study, a bug in the YSU scheme (WRF version 3.3) was discovered (personal communication Heather Richardson, 2012). This bug has been corrected in WRF version 3.4.1 and should result in improved nighttime low-level winds.
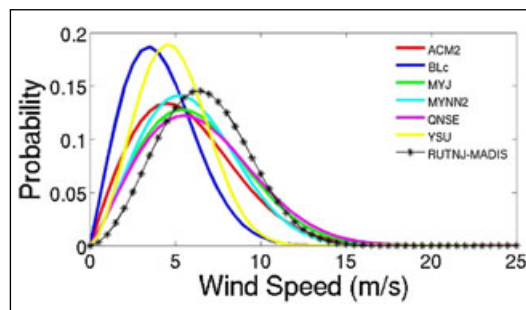
**Figure 6.** Wind speed distribution at 179 m AGL at the RUTNJ site along with modeled wind speed distribution. Distributions are representative of the three days with LLJs present.

**Table II.** Wind Resource Statistics at 179 m AGL. AEP estimates are based on the power curve of the GE 1.5 S model wind turbine with a rotor plane diameter of 70.5 m. A hub height of 179 m was assumed as that was the lowest height of consistently good quality profiler data.

|  | $C$ | $K$ | Mean Wind Speed m/s | Power Density w/m$^2$ | AEP GWh/y |
|---|---|---|---|---|---|
| ACM2 | 6.4096 | 1.9914 | 5.64 | 107.81 | 5.46 |
| Blc | 4.7135 | 2.0789 | 4.16 | 43.30 | 2.08 |
| MYJ | 7.1440 | 2.1901 | 6.32 | 151.12 | 6.88 |
| MYNN2 | 6.7203 | 2.3040 | 5.92 | 124.63 | 5.78 |
| QNSE | 7.3593 | 2.1422 | 6.49 | 164.21 | 7.41 |
| YSU | 5.5070 | 2.5981 | 4.89 | 70.17 | 2.91 |
| Ensemble | 6.3090 | 2.2175 | 5.57 | 110.20 | 5.09 |
| RUTNJ-MADIS | 7.5197 | 2.7574 | 6.70 | 180.10 | 7.39 |

the Weibull scale parameter ($C$) and also demonstrated significant diversity in terms of the shape parameter ($K$).[74] A quantitative assessment of the Weibull parameters, mean wind speed, power density and annual energy production (AEP) error is shown in Table II. AEP estimates are based on the power curve of the GE 1.5 S model wind turbine with a rotor plane diameter of 70.5 m. To avoid extrapolating wind down to the recommended hub height, a hub height of 179 m AGL was assumed as that was the lowest height of consistently good quality profiler data. Power density errors ranged from -8.82% to -75.96% while estimated AEP errors ranged from 0.28% to -71.86%. The multiphysics ensemble AEP estimate had an error of about -30%, which ranks fifth among all other PBL schemes. In addition to potentially offering increased wind resource estimates, the ensemble physics assessments also provide a measure of uncertainty for the expected wind regime. This is provided through the spread in solutions from the ensemble members and can be beneficial for financial risk assessments and planning.

### 4.1.3. Vertical wind shear.

The power law exponent ($\alpha$) is a common metric used to quantify magnitudinal wind shear between two vertical heights AGL. The variable $\alpha$ is defined in the power law equation (Equation (1)) where $Z_1$ is the height of the lower level, $Z_2$ is the height of the upper level and $U$ represents wind speed at each height.

$$\left( \frac{U_{z_2}}{U_{z_1}} \right) \sim \left( \frac{Z_2}{Z_1} \right)^{\alpha} \tag{1}$$

Figure 7 (upper left panel) displays the temporal evolution of $\alpha$ values computed by using $Z_1 = 40$ m and $Z_2 = 140$ m AGL for the LLJ event. Increases in these values up to 1 indicate a highly sheared boundary layer flow. The heights of $Z_1$ and $Z_2$ roughly correspond to typical rotor plane bottom and tip heights of modern offshore wind turbines. As expected, all WRF–PBL schemes modeled an increase in vertical wind shear in association with the formation of each LLJ with $\alpha$ upwards of 0.8 in some cases. Despite these general increases, the degree of $\alpha$ increase varied with each scheme, sometimes by a factor of over two. These differences can likely be attributed to the specific treatment of diffusion, which is unique to each scheme. To put these values in perspective, wind energy developers typically assume values of $\alpha$ between 0.11 and 0.20, which are typically standard for onshore locations[75] and the International Electrotechnical Commission has set wind turbine standards to withstand $\alpha = 0.2$.[76] Obviously, high shear environments such as those induced by the coastal LLJs
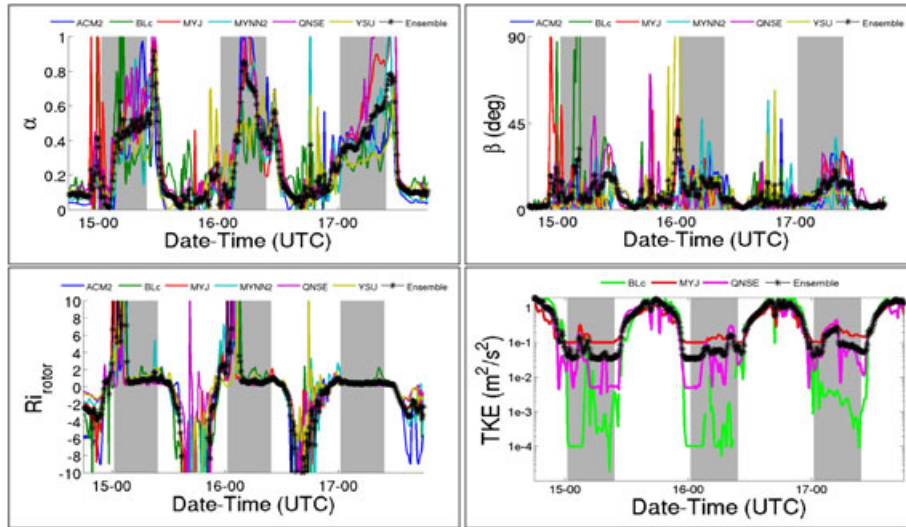
**Figure 7.** WRF model diagnostics corresponding to 40-140m AGL on July 14–17, 2011 at RUTNJ. Areas shading in gray correspond to nighttime hours (00 UTC–09 UTC). Note that *y*-axis in lower right figure is logarithmic.

discussed here will generate unanticipated, enhanced stress on tall turbines.[77] The presence of the three consecutive coastal LLJs also enhanced the simulated absolute directional wind shear ($\beta$) in the WRF model. The variable, $\beta$, is defined as the absolute value of the difference in wind direction between two heights AGL (Equation (2)),

$$\beta = |\phi_{Z_2} - \phi_{Z_1}| \tag{2}$$

where $\phi$ represents wind direction at a specific height ($Z$). The inconsistency between each PBL scheme's physics is highlighted by this parameter as some schemes exhibit minimal directional wind shear whereas others produce directional wind shear over 45 degrees (Figure 7). Nevertheless, a PBL scheme ensemble analysis of this coastal LLJ event clearly illustrates an increase in absolute directional wind shear of about 20 degrees with each jet. Over land, van Ulden and Holtslag[78] estimated the typical value of $\beta$ taken over the entire nighttime stable boundary layer to be $\sim 35°$.

### 4.1.4. Stability.

Another interesting response of the WRF model to the coastal LLJs was evident in $Ri_{\mathrm{rotor}}$, a derivative of the popular Bulk Richardson number.[79] The Bulk Richardson number accounts for atmospheric stability and also vertical wind shear in both horizontal axes throughout the entire boundary layer depth. Negative Bulk Richardson number values indicate a positively buoyant/convective atmosphere, whereas values greater than zero correspond to a stably stratified condition. The variable $Ri_{\mathrm{rotor}}$, which is defined by Equation (3), behaves similarly to the Bulk Richardson number; however, it only considers shear and static stability parameters across the depth of typical wind turbine rotor planes (40–140 m AGL).

$$Ri_{rotor} = \frac{2(Z_2 - Z_1)g}{\theta_{Z_2} + \theta_{Z_1}} \left[ \frac{\theta_{Z_2} - \theta_{Z_1}}{\left(U_{Z_2} - U_{Z_1}\right)^2 + \left(V_{Z_2} - V_{Z_1}\right)^2} \right] \tag{3}$$

In the lower left panel of Figure 7, the diurnal stability cycle of the RUTNJ location is evident by the very negative $Ri_{\mathrm{rotor}}$ values during the afternoon hours and large positive values during the nighttime hours. Additionally, a prolonged period of slightly positive $Ri_{\mathrm{rotor}}$ values corresponds to the presence of each nocturnal LLJ occurrence. This observation supports the hypothesis that coastal LLJs promote boundary layer mixing and reduce nocturnal stability. These results were drawn from the general consensus of all PBL schemes, which were fairly consistent for the majority of each of the LLJ's prevalence. However, variability among schemes was observed both during the afternoon hours and the times when each coastal LLJ was forming.

### 4.1.5. Turbulent kinetic energy.

The WRF model-derived 90 m AGL TKE time series displays small increases in magnitude from 00Z–12Z each night; the times when the LLJ was present (Figure 7 lower right panel). Although dwarfed by the level of turbulence present during

daytime hours, the nocturnal turbulence associated with the presence of the LLJ approaches 0.5 m$^2$/s$^2$ on the final night of simulation. The MYJ PBL scheme demonstrates artificial TKE clipping at 0.1 m$^2$/s$^2$, whereas the BLc scheme maintains a near-zero TKE production environment during nocturnal hours. Also during the nighttime (i.e., the hours when the LLJs are present), simulated TKE is fairly intermittent and characterized by a turbulent bursting type nature. Observations of TKE bursting similar to this has been observed over the US Great Plains in association with onshore LLJs.[16,31,35]

## 4.2. Sensitivity to initial and boundary conditions

Although the primary purpose of this paper is to assess the sensitivity of PBL parameterization on the ability to accurately model coastal LLJs, we similarly investigated the sensitivity of initial and boundary conditions on this accuracy. Surprisingly, we found the ability of the WRF model to capture this LLJ event to be very strongly related to initialization
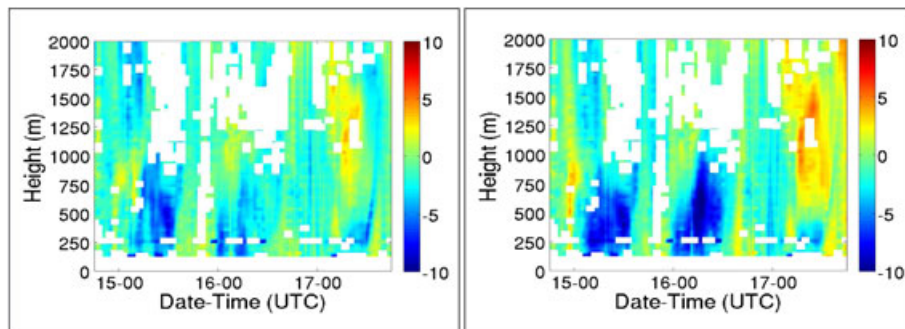


**Figure 8.** Time versus height wind speed difference plot of WRF model derived output minus observations from the RUTNJ MADIS vertical wind profiler by using ERA-Interim (left) and NARR (right) initialization conditions. Data valid for July 14–17, 2011.
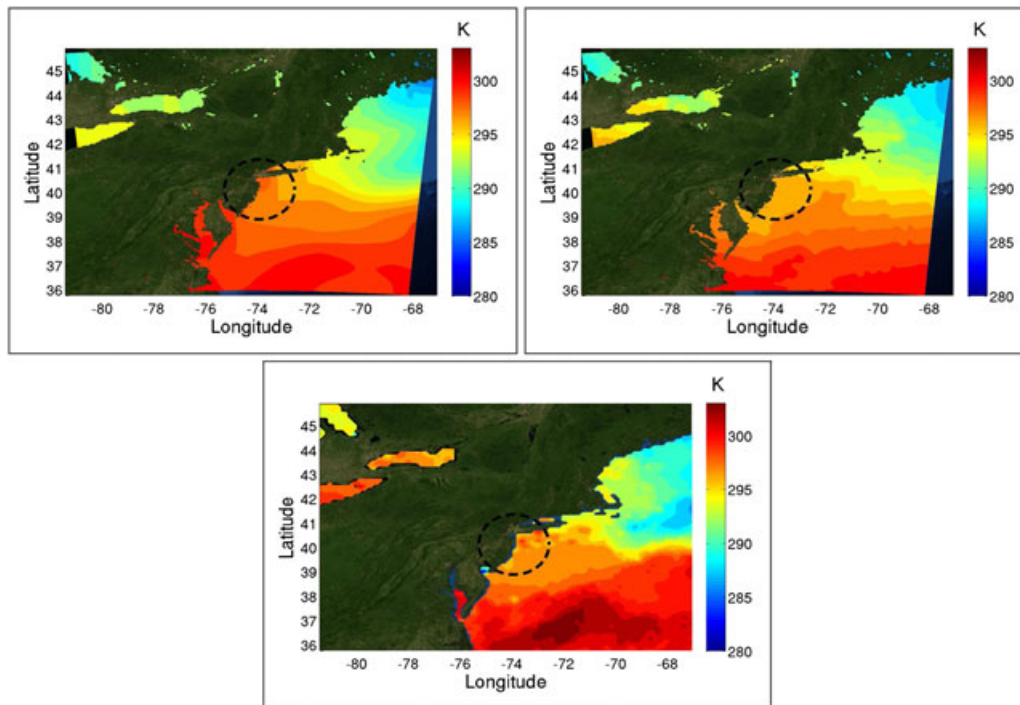


**Figure 9.** Sea surface temperature as modeled by ERA-Interim (top left) and NARR (top right) initialization data sets along with satellite observations from July 17, 2011 (bottom). Observations were derived through composite analysis of data recorded by AVHRR/3, HIRS/3 and HIRS/4 instruments on the NOAA-15, NOAA-17 and NOAA-18 satellites.
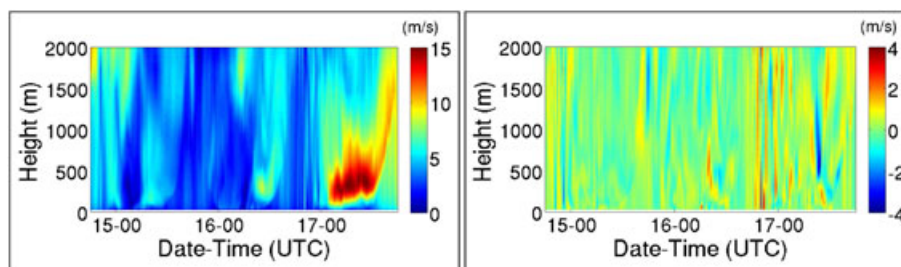
**Figure 10.** Time–height wind speed values for the RUTNJ site using QNSE PBL parameterization and NARR initialization data supplemented by high-resolution satellite-derived SSTs (left). Wind speed difference between original NARR and the NARR supplemented by satellite SSTs (right).

data. To illustrate this connection, the WRF model was run once again by using identical configurations, only this time, by using NARR data for initialization and boundary conditions. In Figure 8, wind speed values from the RUTNJ profiler are subtracted from both the NARR-based simulation and the ERA-Interim-based simulation previously mentioned (both simulations used the QNSE PBL scheme). This time–height comparison clearly show that the performance of the NARR-based simulation was much weaker compared with that of the ERA-Interim with regards to the first two LLJ intensities.

The differences between the data in these two reanalysis are many and associated with multiple model variables. With that being said, it is beyond the scope of this paper to identify the specific parameters responsible for the differences highlighted in Figure 8. Nevertheless, scientifically speaking, these parameters must be related to one or more of the formation and/or amplification mechanisms at play here. Assuming that the primary LLJ development mechanism at work here was that described in Section 2 (i.e., Hsu[50]), two key environmental conditions would be SSTs warmer than the adjacent land surface and weak offshore geostrophic wind.

From satellite observations, it can be seen that SSTs within the innermost modeling domain (d03) were much more heterogeneous than other regions in the vicinity (Figure 9 bottom). On July 17th, multiple warm SST pockets were identifiable offshore of Northern New Jersey and Long Island. The ERA-Interim data better represented this area of warmer water compared with the NARR data set, which was about 1–2 degrees cooler (Figure 9 bottom). Warm SST anomalies, such as those visible in the satellite imagery, may have increased the nocturnal temperature gradient at the coast and thus contributed to LLJ formation. From a modeling perspective, this may have been one of many sources of error that potentially contributed to the poor performance of the NARR-based simulation. To test this speculation, we attempted to improve the weaker NARR-based simulation by incorporating real-time, high-resolution satellite-based SST observations[80] as boundary conditions to the WRF run. Interestingly, this yielded little change in terms of the wind speed vertical profiles throughout the event especially for the first two jets as they went largely unsimulated (Figure 10). This indicates that efforts to improve modeled representation of coastal LLJs by simply addressing individual variables (i.e., SST) may offer little success. An alternative, possibly more helpful tactic from a offshore wind energy standpoint, would be to use a suite of various initialization and boundary conditions to produce modeled wind resource assessments.

## 5. DISCUSSION

In this paper, the implications of coastal LLJs on mesoscale modeling for offshore wind energy applications have been outlined. We have emphasized the importance of accurate initial and boundary conditions for coastal LLJ simulation. In addition, multiple PBL parameterization schemes were evaluated on the basis of their ability to simulate the atmospheric boundary layer with respect to coastal LLJs. For the particular Northeastern US coastal LLJ event studied here, it was acknowledged that multiple processes may have led to its development; however, weak offshore geostrophic forcing combined with significant land–sea temperature differences appeared to be important ingredients.

From a modeling perspective, our results showed that each PBL scheme tended to underestimate the intensity of each jet core while also struggling to capture the presence of the weakest LLJ altogether. On the other hand, the timing of each jet's development and termination was accurately simulated by all PBL schemes. Furthermore, an extraordinary amount of magnitudinal and directional vertical wind shear ($\alpha \sim 1$ and $\beta \sim 20$) was present throughout depths common for wind turbine rotor planes ($\sim$40–140 m AGL). As would be expected, the enhanced vertical wind shear promoted PBL mixing and also led to intermittent bursting of TKE at hub height. Essentially, this degree of inflow heterogeneity has the potential to degrade the structural health of current wind turbines over time.
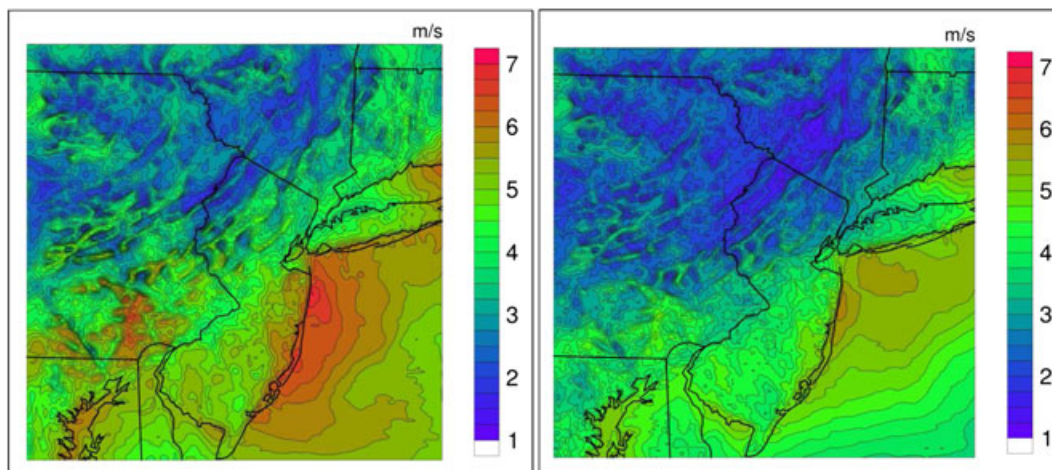
**Figure 11.** 3 day averaged 90 m wind speed as simulated by WRF using MYJ (left) and BLc (right) PBL parameterization schemes. Other than PBL parameterization, all physics, numerics and domain configurations were held constant throughout both simulations.

## 6. FUTURE DIRECTIONS

In a 2011 report,[81] the US Department of Energy (DOE) outlined a national offshore wind strategy for the development of an offshore wind energy infrastructure in the US. In this report, the DOE identified a number of major market barriers. Of these barriers, two important meteorological issues were highlighted: (i) 'the offshore wind resource is not well characterized. This significantly increases uncertainty related to potential project power production and turbine and array design considerations, which in turn increases financing costs' and (ii) 'most meteorological, wave and seabed data used in assessing potential offshore wind sites are based on extrapolations of data from on-shore sites, buoys or limited surveys. The accuracy of these projections has not been properly validated'. Moving forward, the limitation of insufficient offshore meteorological data sets may be addressed in two ways. The first and the most obvious way to address this barrier is to install tall instrumented towers on the US offshore continental shelf in the Gulf of Mexico and in the Great Lakes. The DOE has anticipated that these types of facilities will be 'critical in assessing the costs, energy production, design requirements and overall economic viability of (offshore wind) projects'. Rationally speaking, this is a long-term solution that has already been adopted in Europe (e.g., FINO towers in the North Sea) and Asia; however, it is a financially expensive proposition. An alternative and much more cost-effective way to address the issue of limited offshore data is to use mesoscale models to simulate the expected wind behavior where observations are sparse. This is an attractive solution given the constantly advancing state of high-performance computing and the increasing usability of models such as WRF. Despite the simplicity and efficiency of mesoscale models, the limitations imposed by every physical parameterization along with uncertainty in initial and lateral boundary conditions means that no model will be perfectly accurate as reinforced by this paper. One might speculate that the long-term averaging (say averaging of 365 random day simulations taken from the past decade or so) might reduce or possibly even eliminate the dependence of simulated wind resource climatologies on the model physics parameterizations. Our present study (admittedly, limited in scope) does not support such speculation.* In Figure 11, we compare the 3 day averaged 90 m AGL wind speed from two different model physics options. At some offshore locations, the differences could be as high as 2 m/s. Based on this, we advocate the use of multiphysics ensembles that should provide more accurate wind resource averages and more importantly wind resource uncertainty outlooks.

Even with increased reliance and confidence in mesoscale models, the necessity for tall offshore meteorological towers cannot be ignored as they are desperately needed for model validation. Recently, NREL used ocean buoys, marine automated stations, Coast Guard stations/lighthouses and satellite derived 10 m wind speeds to validate offshore wind maps produced by using a physics-based mesoscale model.[6] 'The wind measurements from these (sources) were extrapolated to 50 m above the surface and compared with the model estimates at the same height by using shear exponents from the Power Law Equation (Elliott *et al.* 1987)'. As emphasized in this paper, this validation technique is compromised by the

---

*A recent mesoscale model intercomparison study,[82] which compared six mesoscale models spanning over a period of 1 year, corroborates our finding (qualitatively). Over the Arctic Ocean, they found that the annual bias of 10 m wind speed among various models ranged from -0.98 m/s to 1.47 m/s.
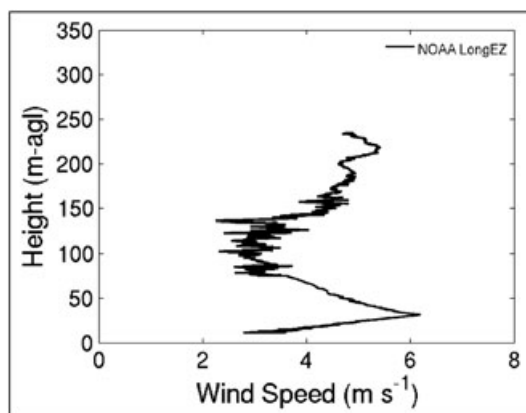
**Figure 12.** Very low LLJ offshore of Martha's Vineyard, MA on August 8, 2001 17UTC. Data measured during the Coupled Boundary Layers/Air–Sea Transfer experiment[83] and provided by Larry Mahrt.

fact that offshore wind regimes may often be characterized by shear exponents much larger than those derived through the Power Law Equation (Equation (1)).

Regardless of the aforementioned data constraints, offshore wind energy remains an attractive avenue of development. However, if mesoscale modeling prevails as an offshore wind resource assessment tool, then it should incorporate new modeling techniques such as four-dimensional data assimilation, coupling to microscale models (e.g., large eddy models) and coupling to ocean wave models. Each of these techniques offers unique benefits that may help to relax erroneous mesoscale model sensitivities, particularly those presented in this paper. Employing these types of new techniques may also prove valuable when attempting to simulate unique coastal atmospheric phenomena with high implications to wind energy. Also, further work should be carried out to climatologically characterize the prevalence and diversity of these phenomena. For example, occurrences of very low LLJs have been observed offshore (Figure 12), yet their frequency and intensity remains largely unknown. To the best of our knowledge, simulations of such phenomena have not been reported in the literature. We expect the ability of conventional mesoscale models to capture events such as this to be extremely weak considering the small scale nature of the phenomena.

## ACKNOWLEDGEMENTS

## APPENDIX A. VERTICAL RESOLUTION SENSITIVITY

Although many components of mesoscale models can contribute the errors identified in this paper, vertical resolution is particularly important for simulations focused on boundary layer flows. For this reason, we present a concise sensitivity study dedicated to understanding the effects of vertical resolution on model accuracy while verifying against the coastal LLJ observational data. To test the effects of vertical resolution, the number of gridpoints in the ABL (i.e., about the lowest 3000 m AGL) were doubled and the coastal LLJ was resimulated (all other modeling configurations identical to those described in Section 3). In Figure A.1, the vertical wind profiles produced by simulations with increased vertical resolution are compared with the baseline simulations presented in Section 4. Two different PBL schemes were chosen for this resolution sensitivity study, one that performed fairly well (QNSE; Figure A.1 left) and another that performed poorly (MYNN2; Figure A.1 right). The quintessential difference between the baseline simulations and the higher resolution simulations is a slightly weaker and slightly lower jet core produced by the higher resolution runs. The increased resolution did not improve the comparably poorer MYNN2 simulation; in fact, it deteriorated the PBL scheme's representation of the LLJ. The same can be said for the QNSE scheme; the result of increasing the vertical resolution only slightly weakened its performance, which was nearly perfect in the baseline simulation.
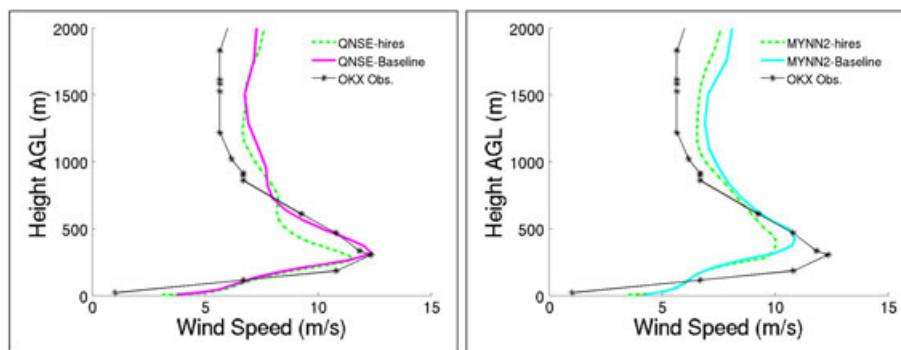
**Figure A.1.** Wind speed as a function of height for the OKX radiosonde launch site. QNSE (left) and MYNN2 (right) modeled profiles are colored and sounding observations are denoted by a line with stars. Data valid on July 17, 2011 12Z.

Nonetheless, these observations are only valid for one time and at one location; nothing can be said regarding the capacity to which these observations can be generalized to describe effects at other locations or times. However, these results do agree with those recently found by Bernier and Bélair[84] who also found increased vertical resolution to not significantly improve or degrade the quality of wind forecasts for wind energy applications. On the other hand, Bernier and Bélair[84] did find that increased vertical resolution may in some cases greatly improve other, more sensitive, model prognostic variables (i.e., moisture fields). Theoretically, an improvement in model representation of these fields should indirectly improve wind representation; however, this improvement is likely insignificant considering the multiple sources of error inherent to mesoscale models. In light of the information presented in this sensitivity study, a justification cannot be made concerning the advantages of increased vertical resolution compared with lower vertical resolution when simulating coastal LLJs. This is especially true given the fact that PBL parameterization has been found to be responsible for much more extreme wind speed errors. On a final note, other model components beyond those assessed in this paper also have the potential to affect the performance of individual PBL schemes such as the lowest gridpoint level AGL.[85]

## REFERENCES

1. Lavagnini A, Semprevia A, Barthelmie R. Estimating wind energy potential offshore in Mediterranean areas. *Wind Energy* 2003; **6**: 23–34.
2. Lange B, Larsen S, Højstrup J, Barthelmie R. The influence of thermal effects on the wind speed profile of the coastal marine boundary layer. *Boundary-Layer Meteorology* 2004; **112**: 587–617.
3. Semprevia A, Barthelmie R, Pryor S. Review of methodologies for offshore wind resource assessment in European seas. *Surveys in Geophysics* 2008; **29**: 471–497.
4. Wilkes J, Moccia J, Arapogianni A, Dragan M, Plytas N, Genachte AB, Guillet J, Wilczek P. The European offshore wind industry key 2011 trends and statistics, 2012. A report by the European Wind Energy Association.
5. Junfeng L, Pengfei S, Hu G, Hongwen X, Zhenbin Y, Wenqian T, Lingjuan M. China wind power outlook, 2010. A report by the Chinese Renewable Energy Industries Association.
6. Schwartz M, Heimiller D, Haymes S, Musial W. Assessment of offshore wind energy resources for the United States. *Technical Report NREL/CP-50045889*, National Renewable Energy Laboratory, 2011.
7. Dvorak M, Corcoran B, Ten Hoeve J, McIntyre N, Jacobson M. US East Coast offshore wind energy resources and their relationship to peak-time electricity demand. *Wind Energy* 2012. DOI: 10.1002/we.1524, (to appear in print). Available at: http://dx.doi.org/10.1002/we.1524.
8. Musial W, Ram B. Large-scale offshore wind power in the United States: Assessment of opportunities and barriers. *NREL/TP-500-40745*, 2010.
9. Dvorak M, Archer C, Jacobson M. California offshore wind energy potential. *Renewable Energy* 2010; **35**: 1244–1254.
10. Barthelmie R, Hansen O, Enevoldsen K, Højstrup J, Frandsen S, Pryor S, Larsen S, Motta M, Sanderhoff P. Ten years of meteorological measurements for offshore wind farms. *Journal of Solar Energy Engineering* 2005; **127**: 170–177.
11. Manwell J, Rogers A, McGowan J, Bailey B. An offshore wind resource assessment study for New England. *Renewable Energy* 2002; **27**: 175–187.
12. Barthelmie R. The effects of atmospheric stability on coastal wind climates. *Meteorological Applications* 1999; **6**: 39–47.

13. Buckley RL, Kurzeja RJ. An observational and numerical study of the nocturnal sea breeze. Part I: structure and circulation. *Journal of Applied Meteorology* 1997; **36**: 1577–1598.

14. Barthelmie R, Badger J, Pryor S, Hasager C, Christiansen M, Jørgensen B. Offshore coastal wind speed gradients: issues for the design and development of large offshore windfarms. *Wind Engineering* 2007; **31**: 369–383.

15. Mahrt L, Vickers D, Moore E. Flow adjustments across sea-surface temperature changes. *Boundary-Layer Meteorology* 2003; **111**: 553–564.

16. Banta R, Newsom R, Lundquist J, Pichugina Y, Coulter R, Mahrt L. Nocturnal low-level jet characteristics over Kansas during CASES-99. *Boundary Layer Meteorology* 2002; **105**: 221–252.

17. Pichugina YL, Banta RM, Kelley ND, Sandberg SP, Machol JL, Brewer WA. Nocturnal low-level jet characteristics over Southern Colorado. In *Preprints, 16th Symp. On Boundary Layers and Turbulence*, Vol. 4. Portland, ME, American Meteorological Society, CD-ROM, 2004.

18. Helfand H, Schubert SD. Climatology of the simulated Great Plains low-level jet and its contribution to the continental moisture budget of the United States. *Journal of Climate* 1995; **8**: 784–806.

19. Higgins R, Yao Y, Yarosh E, Janowiak J, Mo K. Influence of the Great Plains low-level jet on summertime precipitation and moisture transport over the central United States. *Journal of Climate* 1997; **10**: 481–507.

20. Berg LK, Zhong S. Sensitivity of MM5 simulated boundary-layer characteristics to turbulence parameterization. *Journal of Applied Meteorology and Climatology* 2005; **44**: 1467–1483.

21. Miao J, Chen D, Wyser K, Borne K, Lindgren J, Strandevall MKS, Thorsson S, Achberger C, Almkvist E. Evaluation of MM5 mesoscale model at local scale for air quality applications over the Swedish West Coast: influence of PBL and LSM parameterizations. *Meteorology and Atmospheric Physics* 2008; **99**: 77–103.

22. Storm B, Dudhia J, Basu S, Swift A, Giammanco I. Evaluation of the weather research and forecasting model on forecasting low-level jets: implications for wind energy. *Wind Energy* 2008; **12**: 81–90.

23. Schmidli J, Billings B, Chow FK, de Wekker SFJ, Doyle J, Grubii V, Holt T, Jiang Q, Lundquist KA, Sheridan P, Vosper S, Whiteman CD, Wyszogrodzki AA, Zängl G. Intercomparison of mesoscale model simulations of the daytime valley wind system. *Monthly Weather Review* 2011; **139**: 1389–1409.

24. Shin HH, Hong S. Intercomparison of planetary boundary-layer parameterizations in the WRF model for a single day from CASES-99. *Boundary-Layer Meteorology* 2011; **139**: 261–281.

25. Jones M, Colle B, Tongue J. Evaluation of a mesoscale short-range ensemble forecast system over the northeast United States. *Weather and Forecasting* 2007; **22**: 36–55.

26. Bonner W. Climatology of the low level jet. *Monthly Weather Review* 1968; **96**: 833–850.

27. Whiteman CD, Bian X, Zhong S. Low-level jet climatology from enhanced rawinsonde observations at a site in the Southern Great Plains. *Journal of Applied Meteorology* 1997; **36**: 1363–1376.

28. Song J, Liao K, Coulter R, Lesht B. Climatology of the low-level jet at the southern Great Plains atmospheric boundary layer experiments site. *Journal of Applied Meteorology and Climatology* 2005; **44**: 1593–1606.

29. Andreas E, Claffy K, Makshtas A. Low-level atmospheric jets and inversions over the Western Weddell Sea. *Boundary-Layer Meteorology* 2000; **97**: 459–486.

30. Banta R, Pichugina Y, Kelley N, Jonkman B, Brewer W. Doppler lidar measurements of the Great Plains low-level jet: applications to wind energy. *IOP Conference Series: Earth and Environmental Science* 2008; **1**. DOI: 10.1088/1755-1315/1/1/012020.

31. Banta R. Stable-boundary-layer regimes from the perspective of the low-level jet. *Acta Geophysica* 2008; **56**: 58–87.

32. Sisterson D, Frenzen P. Nocturnal boundary-layer wind maxima and problem of wind power assessment. *Environmental Science and Technology* 1978; **12**: 218–221.

33. Zhou B, Chow F. Turbulence modeling for the stable atmospheric boundary layer and implications for wind energy. *Flow, Turbulence and Combustion* 2012; **88**: 255–277.

34. Poulos G, Blumen W, Fritts D, Lundquist J, Sun J, Burns S, Nappo C, Banta R, Newsom R, Cuxart J, Terradellas E, Balsely B, Jensen M. CASES 99 – a comprehensive investigation of the stable nocturnal boundary layer. *Bulletin of the American Meteorological Society* 2002; **83**: 555–581.

35. Kelley N, Jonkman B, Scott G. The Great Plains turbulence environment: its origins, impact and simulation. *Technical Report NREL/CP-50040176*, National Renewable Energy Laboratory, 2006.

36. Wharton S, Lundquist J. Atmospheric stability affects wind turbine power collection. *Environmental Research Letters* 2012; **7**. DOI: 10.1088/1748-9326/7/1/014005.

37. Blackadar K. Boundary layer wind maxima and their significance for the growth of nocturnal inversions. *Bulletin of the American Meteorological Society* 1957; **38**: 283–290.

38. Parish T, Oolman L. On the role of sloping terrain in the forcing of the Great Plains low-level jet. *Journal of the Atmospheric Sciences* 2010; **67**: 2690–2699.

39. Van de Wiel B, Moene A, Steeneveld G, Baas P, Bosveld F, Holtslag A. A conceptual view on inertial oscillations and nocturnal low-level jets. *Journal of the Atmospheric Sciences* 2010; **67**: 2679–2689.

40. Kottmeier C, Palacio-Sese P, Kalthoff N, Corsmeier U, Fiedler F. Sea breezes and coastal jets in Southeastern Spain. *International Journal of Climatology* 2000; **20**: 1791–1808.

41. Mitchell MJ, Arritt RW, Labas K. A climatology of the warm season Great Plains low-level jet using wind profiler observations. *Weather and Forecasting* 1995; **10**: 576–591.

42. Baas P, Bosveld FC, Baltink HK, Holtslag AAM. A climatology of nocturnal low-level jets at Cabauw. *Journal of Applied Meteorology and Climatology* 2009; **48**: 1627–1642.

43. Liu S, Liang X. Observed diurnal cycle climatology of planetary boundary layer height. *Journal of Climate* 2010; **23**: 5790–5809.

44. Smedman A, Bergström H, Högström U. Spectra, variances and length scales in a marine stable boundary layer dominated by a low level jet. *Boundary-Layer Meteorology* 1995; **76**: 211–232.

45. Doyle J, Warner T. A Carolina coastal low-level jet during GALE IOP 2. *Monthly Weather Review* 2010; **138**: 2385–2404.

46. Zhang D, Zhang S, Weaver S. Low-level jets over the Mid-Atlantic states: a warm season climatology and a case study. *Journal of Applied Meteorology and Climatology* 2006; **45**: 194–209.

47. Colle B, Novak D. The New York Bight jet: climatology and dynamical evolution. *Monthly Weather Review* 2010; **138**: 2385–2404.

48. Jiang Q, Wang S, O'Neill L. Some insights into the characteristics and dynamics of the Chilean low-level coastal jet. *Monthly Weather Review* 2010; **138**: 3185–3206.

49. Kraus H, Malcher J, Schaller E. A nocturnal low level jet during PUKK. *Boundary-Layer Meteorology* 1985; **31**: 187–195.

50. Hsu S. Mesoscale nocturnal jetlike winds within the planetary boundary layer over a flat, open coast. *Boundary-Layer Meteorology* 1979; **17**: 485–495.

51. Hsu S. Coastal air-circulation system: observations and empirical model. *Monthly Weather Review* 1970; **98**: 487–509.

52. Hull L, Dannevik W, Woodford R. Meteorological analysis for the Anclote Keys Plume Study. *Technical Report 68-02-2500*, Atmospheric Chemistry and Physics Division, Environmental Protection Agency, 1979.

53. Rife D, Pinto J, Monaghan A, Davis C. Global distribution and characteristics of diurnally varying low-level jets. *Journal of Climate* 2010; **23**: 5041–5064.

54. Ryan WF. The low level jet in Maryland: profiler observations and preliminary climatology. *Technical Report*, Maryland Department of the Environment, Air and Radiation Administration, 2004.

55. Piety CA. Radar wind profiler observations in Maryland: a preliminary climatology of the low level jet. *Technical Report*, Maryland Department of the Environment, Air and Radiation Administration, 2005.

56. National Weather Service Office of Systems Development. Technique specification package 88-21-R2 for AWIPS-90 RFP Appendix G Requirements numbers: quality control incoming data. *Technical Report*, National Oceanic and Atmospheric Administration, 2004.

57. Skamarock WC, Klemp JB, Dudhia J, Gill DO, Barker DM, Duda MG, Huang XY, Wang W, Powers JG. A description of the advanced research WRF version 3. *Technical Report NCAR/TN-457+STR*, National Center for Atmospheric Research, 2008.

58. Hong S, Noh Y, Dudhia J. A new vertical diffusion package with an explicit treatment of entrainment processes. *Monthly Weather Review* 2006; **134**: 2318–2341.

59. Janjìc ZI. The step-mountain eta coordinate model: further developments of the convection, viscous sublayer, and turbulence closure schemes. *Monthly Weather Review* 1994; **122**: 927–945.

60. Sukoriansky S, Galperin B, Perov V. Application of a new spectral theory of stably stratified turbulence to the atmospheric boundary layer over sea ice. *Boundary-Layer Meteorology* 2005; **117**: 231–257.

61. Nakanishi M, Niino H. An improved Mellor–Yamada level 3 model: its numerical stability and application to a regional prediction of advection fog. *Boundary-Layer Meteorology* 2006; **119**: 397–407.

62. Pleim JE. A combined local and nonlocal closure model for the atmospheric boundary layer. Part I: model description and testing. *Journal of Applied Meteorology and Climatology* 2007; **46**: 1383–1395.

63. Pleim JE. A combined local and nonlocal closure model for the atmospheric boundary layer. Part II: application and evaluation in a mesoscale meteorological model. *Journal of Applied Meteorology and Climatology* 2007; **46**: 1396–1409.

64. Bougeault P, Lacarrère P. Parameterization of orography-induced turbulence in a mesobeta-scale model. *Monthly Weather Review* 1989; **117**: 1872–1890.

65. Hong SY, Dudhia J, Chen SH. A revised approach to ice microphysical processes for the bulk parameterization of clouds and precipitation. *Monthly Weather Review* 2004; **132**: 103–120.

66. Mlawer E, Taubman S, Brown P, Iacono M, Clough S. Radiative transfer for inhomogeneous atmosphere: RRTM, a validated correlated-k model for the longwave. *Journal of Geophysical Research* 1997; **102**: 16 663–16 682.

67. Dudhia J. Numerical study of convection observed during the winter monsoon experiment using a mesoscale two-dimensional model. *Journal of the Atmospheric Sciences* 1989; **46**: 3077–3107.

68. Kain J. The Kain–Fritsch convective parameterization: an update. *Journal Applied Meteorology* 2004; **43**: 170–181.

69. Chen F, Dudhia J. Coupling an advanced land-surface/hydrology model with the Penn State/NCAR MM5 modeling system. *Monthly Weather Review* 2001; **129**: 587–604.

70. Potter CW, Debra L, McCaa J, Cheng S, Eichelberger S, Grimit E. Creating the dataset for the western wind and solar integration study (USA). *Wind Engineering* 2008; **32**(4): 325–338.

71. Global forecast system documentation version 9.0.1. [Online]. Available: http://www.emc.ncep.noaa.gov/GFS/doc.php. (Accessed 03 April 2012) from the National Centers for Environmental Prediction.

72. Berrisford P, Dee D, Fielding K, Fuentes M, Kallberg P, Kobayashi S, Uppala S. The ERA-Interim archive. *Technical Report*, ECMWF, 2009. ERA Report Series, No.1.

73. North American Regional Reanalysis documentation. [Online] Available: http://www.emc.ncep.noaa.gov/mmb/rreanl/. (Accessed: 09 September 2012) from the National Centers for Environmental Prediction.

74. Mathew S, Jansen BJ. *Wind Energy: Fundamentals, Resource Analysis and Economics*, Vol. 1. Springer Heidelberg, 2006.

75. Emeis S. *Wind Power Meteorology*. Springer–Verlag: Berlin/Heidelberg, 2013.

76. IEC. Wind turbine generator system part 1: Design requirements, 3rd ed. *Technical Report IEC 61400-I*, International Electrotechnical Commission, 2005.

77. Giebel G, Gryning S. Shear and stability in high met masts, and how WAsP treats it. The science of making torque from wind. *Technical Report*, European Wind Energy Association, 2004.

78. van Ulden A, Holtslag A. Estimation of atmospheric boundary layer parameters for diffusion applications. *Journal of Climate and Applied Meteorology* 1985; **24**: 1196–1207.

79. Stull RB. *An introduction to boundary layer meteorology*. Kluwer Academic Publishers: Dordrecht, The Netherlands, 1988.

80. Real-time, global, sea surface temperature analysis documentation. [Online] Available: http://polar.ncep.noaa.gov/sst/rtg_high_res/. (Accessed: 20 November 2012) from the National Centers for Environmental Prediction.

81. DOE. A national offshore wind strategy creating an offshore wind energy industry in the United States. *Technical Report DOE/GO-102011 -2988*, United States Department of Energy, 2011.

82. Tjernström M, Žagar M, Svensson G, Cassano JJ, Pfeifer S, Rinke A, Wyser K, Dethloff K, Jones C, Semmler T, Shaw M. Modelling the Arctic boundary layer: an evaluation of six ARCMIP regional-scale models using data from The Sheba Project. *Boundary-Layer Meteorology* 2004; **117**: 337–381.
Tjernström M, Őagar M

83. Edson J, Crawford T, Crescenti J, Farrar T, French J, Frew N, Gerbi G, Helmis C, Hristov T, Khelif D, Jessup A, Jonsson H, Li M, Mahrt L, McGillis W, Plueddemann A, Shen L, Skyllingstad E, Stanton T, Sullivan P, Sun J, Trowbridge J, Vickers D, Wang S, Wang Q, Weller R, Wilkin J, Williams A, Yue DKP, Zappa C. The coupled boundary layers and air–sea transfer experiment in low winds (CBLAST-Low). *Bulletin of the American Meteorological Society* 2007; **88**: 341–356.

84. Bernier N, Bélair S. High horizontal and vertical resolution limited-area model: near-surface and wind energy forecast applications. *Journal of Applied Meteorology and Climatology* 2012; **51**: 1061–1078.

85. Shin H, Hong S, Dudhia J. Impacts of the lowest model level height on the performance of planetary boundary layer parameterizations. *Monthly Weather Review* 2012; **140**: 664–682.